Journal of Applied Electrochemistry **31**: 137–144, 2001.

Pulse plating of cobalt–iron–copper alloys

P.E. BRADLEY[1], B. JANOSSY[2] and D. LANDOLT[1]*
[1]*Laboratoire de Métallurgie chimique, Département des Matériaux, Ecole Polytechnique Fédérale de Lausanne, CH-1015 Lausanne EPFL, Switzerland*
[2]*Institut de Microsystèmes, Département de Microtechnique, Ecole Polytechnique Fédérale de Lausanne, CH-1015, Switzerland*
*(*author for correspondence)*

Received 30 May 2000; accepted in revised form 15 August 2000

Key words: alloy plating, inverted rotating disc electrode, magnetic alloys, pulse plating

Abstract

Pulse plating of cobalt–iron–copper (CoFeCu) alloys was studied. A simple theoretical model with an analytical solution developed for binary alloys is applied to predict the copper content of the pulse plated ternary alloys. Studied compositions are in the range of $Co_{90-x}Fe_{10}Cu_x$ with x varying between 5 to 20 wt %. These compositions are of interest as soft magnetic materials with high saturation magnetization. The deposits were produced from a boric acid and sodium acetate electrolyte with low concentrations of copper and iron. All experiments were carried out under well-controlled mass transport conditions and current distribution using a recessed rotating cylinder electrode (rRCE) or an inverted rotating disc electrode (IrRDE). With the latter design alloys can be plated on flat substrates with or without application of a magnetic field to induce uniaxial magnetic anisotropy. Results show that by changing pulse parameters one can increase and decrease in opposite ways the copper and the iron content in the deposits. To test the influence of pulse parameters on the coercive field strength, a microstructure dependent property, theoretical predictions were used to produce films of identical composition with different pulse parameters. Within the range of pulse parameters studied the coercive field strength of this alloy does not vary. Transmission electron microscopy confirms that the deposits have the same nano-size grain structure.

1. Introduction

Soft magnetic thin films with high saturation magnetization manufactured by electroplating present a growing interest driven by the commercial potential of microdevices manufactured by integrated processing techniques. To this regard, electroplating is of particular interest at an industrial level for low cost and ease of operation. Two critical parameters that allow for soft magnetic properties are low or vanishing magnetocrystalline anisotropy and magnetostriction. These two conditions are however hard to satisfy simultaneously. Such is the case for FeNi alloys with 80 wt % nickel and 20 wt % iron (Permalloys), but their saturation magnetization is only 0.8 T. Other crystalline phases with higher saturation magnetization (B_s) that are of interest for microcomponents satisfy either one or the other of the above quoted criteria. FeNi at 50/50 wt % satisfies near zero magnetocrystalline anisotropy with a B_s of 1.2 T and CoFe at 45/55 wt % can satisfy near zero magnetostriction with a $B_s > 2.0$ T [1]. CoFe at 90/10 wt % has near zero magnetostriction with a B_s of 1.9 T [1–4]. A composition line of near zero magnetostriction exists also for the CoFeNi system [4].

It has been observed in bulk materials that as soon as the structural correlation length or grain size becomes smaller than the ferromagnetic exchange length the coercive field strength decreases drastically [5]. A decrease of the magnetic coercive field strength when the grain size reaches the nanometer scale has been observed also in thin films [6, 7]. Nanocrystalline phases allow for interesting soft magnetic properties from a wide variety of alloy compositions even if the corresponding macrocrystalline phases satisfy only one of the above quoted criteria. The first breakthrough in thin film electroplating of soft magnetic alloys with a high saturation magnetization ($B_s > 1.2$ T) was achieved with high cobalt CoNiFe alloys [8]. Non-magnetostrictive compositions of CoFeNi thin films were first obtained using vacuum deposition [4]. High moment CoFe thin films fabricated by electrodeposition [2, 3, 9] revealed the possibility of achieving vanishing magnetostriction in CoFe alloys with 90 wt % Co at the phase boundary between f.c.c. and b.c.c. The interest for these high cobalt alloys lead to a set of studies trying to optimize their properties by using different metallic or nonmetallic additives. Among other effects, the additives critically

affect the resulting grain size, which in turn strongly influences the coercive field strength (H_c) of the soft magnetic thin films. Although B_s is an intrinsic material property that is directly determined by the alloy composition, H_c is a structure dependent property that can be optimized by subtle changes in bath composition or processing technique. The addition of boron from a reducing agent to produce CoFeB thin films [10], and addition of thiourea instead of saccharin for the CoFeNi system [11, 12] are examples of the use of nonmetallic additives. The work on electroplated CoFe in the presence of saccharin [9] followed by the study of the CoFeCu system [13–16] illustrates the role that a third alloying element can play for the improvement of soft magnetic properties resulting, among other effects, from a reduction of the grain size. Addition of boron to this ternary system to improve material properties such as the corrosion resistance was also investigated [17]. Studies of the CoFeNi mixed b.c.c. and f.c.c. crystalline phase boundaries with and without organic additives [18–20] confirm the importance of alloying for the grain size of deposits and their soft magnetic properties. Addition of chromium to CoFe alloys in combination with pulse-current processing yielded soft magnetic properties with improved corrosion resistance and higher electrical resistivity for high frequency applications [20, 21].

Previously, pulse plating of binary CuNi [22–25] and CuCo [26, 27] alloys has been studied in our laboratory. Pulse parameters were found to have a strong influence on the composition and growth morphology of CuCo alloys [26, 27]. It was therefore considered of interest to apply the same principles to pulse plating of a ternary alloy such as CoFeCu that is of interest for its soft magnetic properties. The present study is aimed at the exploration of the influence of pulse parameters on the resulting alloy composition and on the coercive field strength, a structure sensitive magnetic property.

2. Theoretical models for pulse plating of alloys

Previous studies on pulse plating of binary alloys from solutions containing a low ionic concentration of a noble metal and a large concentration of a less noble metal showed that under certain assumptions the composition of binary alloys can be theoretically predicted. Only mass transport properties of the more noble element in the electrolyte are needed for the calculation of its fraction in the deposits [22, 25]. The same approach is applied here to the prediction of concentration in the ternary alloy CoFeCu which will be treated as a pseudo binary system with copper as the noble element and CoFe as the less noble elements. Application of the corrosion model introduced by Roy et al. [22] to the present alloy system yields for the copper content:

$$X_{Cu} = \frac{i_{lim,Cu}(t_p + t'_p)}{i_p t_p + i'_p t'_p} \tag{1}$$

where X_{Cu} (mol %) is the mol fraction of copper in the deposit, $i_{lim,Cu}$ is the limiting current density of copper, t_p and t'_p are the pulse on-time and pulse off-time, respectively, and i_p, i'_p are the corresponding applied current densities. The model assumes that during the pulse off-time copper ions spontaneously react at their limiting current with the less noble elements in a displacement reaction. The model has been shown to be valid for short pulse off-times [22] as long as the displacement reaction is not slowed down by a decrease in corroding surface area caused by increasing surface coverage of the depositing copper. In deriving Equation 1 the current efficiency for alloy deposition is assumed to be 100%. In the present case, due to the presence of Fe, the current efficiency for alloy deposition is usually less than 100%. It can be shown easily that when copper deposits at limiting current with 100% efficiency and the overall current efficiency for alloy deposition is γ, the copper mol fraction in the alloy is given by Equation 2

$$X_{Cu} = \frac{i_{lim,Cu}(t_p + t'_p)}{\gamma i_p t_p + i'_p t'_p} \tag{2}$$

For the electrolyte solution considered in this work, the charge number is the same ($z = 2$) for Co, Fe and Cu. The current efficiency for alloy deposition therefore is

$$\gamma = \frac{Q_{dep}}{Q_{appl}} = \frac{zFm}{Q_{appl}} \sum_k \frac{X_k^{mass}}{M_k} \tag{3}$$

where $Q_{appl} = n_{cycl}\ (I_p t_p + I'_p t'_p)$ is the total charge applied during n_{cycl} pulse cycles. The charge consumed for depositing the alloy is Q_{dep} and m is the mass of the deposit. X_k^{mass} is the mass fraction and M_k is the molar mass of component k (k = Co, Fe, Cu). I_p is the pulse current and I'_p is the pulse-off current. The other symbols have their usual meaning. Equation 2 permits to calculate the copper content of pulse plated alloys from knowledge of the limiting current of copper and of the overall current efficiency for alloy deposition. The latter has to be determined experimentally which limits somewhat the predictive character of the model.

3. Experimental details

3.1. *Electrolyte*

The formulation of the electrolyte given in Table 1 is based on the literature [13, 15]. The pH of the electrolyte was pH $\sim$ 3.6. The preparation of the solution proceeded by first dissolving Co, Cu, boric acid, Na-acetate and saccharine, with short heating and cooling, addition of H_2SO_4 and completion to one litre. The solution was

Table 1. Formulation of CoFeCu plating electrolyte

Concentrations	Chemical species
0.3 M	$CoSO_4 \cdot 7\ H_2O$
0.025 M	$FeSO_4 \cdot 7\ H_2O$
0.025 M	$CuSO_4 \cdot 5\ H_2O$
0.4 M	H_3BO_3
0.1 M	CH_3COONa
2.0 g l^{-1}	Saccharine ($C_7H_4NNaSO_3S \cdot 2\ H_2O$)
0.2 g l^{-1}	SDS (sodium dodecylsulfate)
28 ml l^{-1}	H_2SO_4 1.5 M

then transferred to the cell and sparged strongly with nitrogen for 30 min. Finally Fe and SDS were added. The described procedure limited the oxidation of ferrous to ferric ions, and avoided excessive production of foam.

3.2. *Electrode geometry, materials and cell design*

Rotating cylinder and rotating disc electrodes were used. A conventional rotating gold disc electrode with a diameter of 3 mm was used for the characterization of mass transport of copper species. Plating experiments were carried out on a recessed rotating cylinder electrode (rRCE) or on a recessed inverted rotating disc electrode (IrRDE) [26–29]. The aspect ratio defined as recess height over the half length of the cylinder electrode or the radius of the disc was 0.5. This value was chosen to achieve relative uniformity of the current distribution while limiting border effects on mass transport [26]. The 8 mm diameter disc electrodes had a surface area of 0.50 cm^2 and the recess height was 2.0 mm. The 10 mm diameter cylinder electrodes of 12.8 mm length had a surface area of 4.02 cm^2 and a recess height of 3.2 mm. Both electrode geometries allowed for easy evacuation of gas bubbles during plating [26, 28, 29]. To limit pollution of the electrolyte at the cathode, all experiments were carried out with a counter electrode separated by a glass frit [26]. The rRCE were made of pure silver (99.95%) polished to a 1 μm near mirror finish. Disc electrodes for plating experiments were made from 1.4 cm^2 cuts of '3 inch' n-phosphorous doped Si (1 1 1) wafers with a resistivity of 0.002 Ω cm. Sputtered titanium served an adhesion layer for the sputter deposited silver film used as cathode. Contact on the back side of the wafer was achieved with quick drying silver paint (Agar Scientific Ltd, Essex, England). Silver was chosen as a cathode material because it has no superimposed X-ray fluorescence signal with Co, Fe, and Cu and it has a relatively low exchange current density for hydrogen. Also, the bulk silver electrodes could be reused after anodic dissolution of the deposits. Details on substrate preparation and recycling of electrodes have been given elsewhere [26, 27].

3.3. *Polarization experiments*

Quasi-steady state polarization curves were measured on flat gold rotating disc electrodes to determine the limiting current of copper in the CoFeCu plating bath. A computer-driven potentiostat/galvanostat (AutoLab, Eco Chemie, Holland) with commercial software and autoranging facility was used. The potential was varied from $E = -0.4$ to -1.4 V vs MSE with a sweep rate of 5 mV s^{-1}. To obtain reproducible results at low potentials a series of preliminary polarization sweeps was carried out on the gold substrate until the currents became reproducible. This usually occurred when the gold became covered with copper. Reproducible polarization curves at different rotation rates could then be measured while the surface of the disc remained mirror like. After experiments the deposits were dissolved in a diluted HNO_3 solution and the electrode was reused.

3.4. *Pulse plating experiments*

Pulse-current experiments were carried out with a computer driven potentiostat/galvanostat PG 390 (Heka-Elektronik, 67466 Lambrecht Germany). The differential amplifier characteristics of this instrument permits the continuous generation of pulses with an excellent squareness. Details of the experimental set-up have been described elsewhere [26, 27]. Three series of experiments with different pulse parameters were performed as shown in Table 2. The first set of experiments was aimed at observing the effect of the displacement reaction on the copper, cobalt and iron content in the deposits. These experiments were carried out with the rRCE using a fixed pulse on-time and varying pulse off-time. Subsequent experiments were carried out with the IrRDE. The experimental series 2 of Table 2 at fixed duty cycle was aimed at obtaining alloys of constant composition for different applied pulse parameters in order to observe their effect on the structure sensitive coercive field strength. Series 3 was similar except that a magnetic field was applied during plating and that the rotation rate was lower. Two magnets were embedded in the sample holder and positioned under the silicium wafer (Figure 1) to induce a uniaxial magnetic anisot-

Table 2. Experimental conditions for pulse plating experiments

Series electrode	Duty cycle	t_p /ms	t'_p /ms	I_p /mA	I'_p /mA	A_{cyl} /cm^2	ω /rpm	$I_{lim,Cu}$ /mA cm^{-2}
1 rRCE	var.	40	10, 40, 60, 100, 160, 320	−220	−0.18	4.02	1000	−2.11
2 IrRDE	0.2	var.	16, 80, 160, 400, 1600	−22.2	−0.79	0.5	238	−2.00
3 IrRDE	0.2	var.	16, 80, 160, 400, 1600	−22.2	−0.39	0.5	60	−1.00

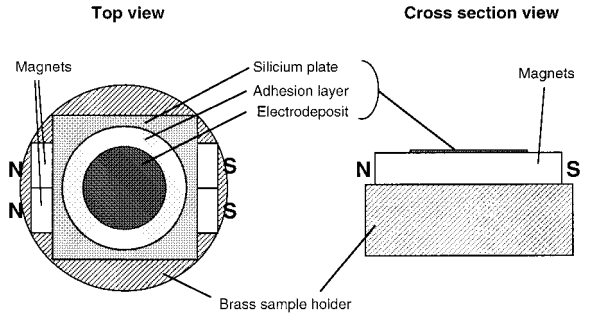

Fig. 1. Schematic representation of substrate, sample holder and magnet arrangement to induce a uniaxial magnetic anisotropy in the electrodeposited films plated with the IrRDE. N and S are respectively the north and the south poles of the magnets.

ropy in the electrodeposits. The assembly was held together using silver conducting paste to guarantee a good electrical contact of the doped silicium substrate with the sample holder.

3.5. *Characterization of deposits*

The current efficiency was determined by gravimetry using the larger surface area rRCE. A precision balance (Sartorius model 2004 MP6, Instrumenten Gesellschaft AG) was used to measure the weight gain to better than 1.0% for films thicker than 1 μm. The composition of the deposits was determined by X-ray fluorescence (XRF) using a Kevex Omicron model 954 with a 300 μm source collimator. Average compositions were determined from seven measurements along the length of the cylinder. For the determination of the alloy composition on disc electrodes five measurements along the diameter of the disc were averaged, avoiding the near edge area. All alloy compositions in the present paper are given in mol %.

3.6. *Magnetic set-up and instruments*

A laboratory made alternating field inductive magnetometer was used for measuring *B–H* loops. A uniform field is produced by a solenoid excited with an alternating sinusoidal current. A sensing coil composed of two coils wound in opposing polarity is positioned near the film inside the primary coil. The two sensing coils compensate each other and this results in zero signal in the absence of a sample. When a sample is introduced in one of the coils, an induced voltage is produced proportional to the rate of change of magnetization integrated over the cross-sectional area of the film

$$\frac{\mathrm{d}}{\mathrm{d}t}\left(\int_{\text{area}} \mu_0 M \mathrm{d}A\right) \tag{4}$$

Integration of this signal returns the magnetic flux ϕ of the magnetization M. For our set-up, sensing coils were not calibrated. However, the saturation magnetization for $Co_{90-x}Fe_{10}Cu_x$ alloys are known from the literature for $x = 5$ and $x = 10$ to be 20 and 18 kG, respectively [15]. The exciting solenoid was calibrated with a hall sensor. A magnetic field of 7.8 Oe was measured for a 0.150 A current. A Hewlett Packard 33120A 15 MHz arbitrary waveform generator was used as a source, the applied sinusoidal current at 1 kHz is converted in units of applied field by measuring the voltage over an ohmic resistance of 10 Ω (Oersted $\equiv$ voltage $\times$ 7.8/(0.15 $\times$ 10)). A differential low noise preamplifier model SR560 from Stanford Research Systems was connected to the pick-up coils, and an oscilloscope Tektronix TDS 420A was used to record the signals. The acquired data were treated with Microcal Origin® software to integrate the measured data and determine the coercive field strength, H_c, from *B–H* magnetic loop hysteresis.

4. Results

4.1. *Mass transport of copper ions*

Current–potential curves were measured on flat rotating disc electrodes for determining the limiting current of copper in the plating bath. To evaluate the limiting current under conditions where no distinct plateau could be measured because of codeposition reactions the Koutecki–Levich Equation 5 was used [30, 31]:

$$\frac{1}{i} = \frac{1}{i_k} + \frac{1}{i_{lim}} = \frac{1}{i_k} + \left(\frac{1}{b_{RDE}}\right)\frac{1}{\omega^{0.5}} \tag{5}$$

The limiting current density is

$$i_{lim} = (b_{RDE})\omega^{1/2} \tag{6}$$

with $b_{RDE} = 0.62\, nFC_bD^{2/3}\nu^{-1/6}$.

Figure 2 shows quasi-steady state polarization curves measured at the RDE and Table 3 shows the results of regression analysis for different potential ranges. The results are very close to each other. The slightly higher values for the limiting current at the most cathodic potentials is attributed to hydrogen evolution. The begin of hydrogen evolution can be detected on the measured current signal by the noise generated by gas bubbles. The most reliable value for the limiting current density of copper obtained at the lowest potentials at which reproducible kinetic conditions can be achieved corresponds to a value of $b_{RDE} = 0.4 \times 10^{-3}$ A cm^{-2} - rad$^{-1/2}$.

4.2. *Pulse-current plating experiments*

The first set of pulse plating experiments was carried out with the rRCE. Previous studies had shown that on disc and cylinder electrodes the recess affects mass transport conditions only near the edge of the electrode, the remainder 80–90% of the surface being not affected. Composition measurements by XRF were carried out in the unaffected regions only. Using Equation 2 the pulse

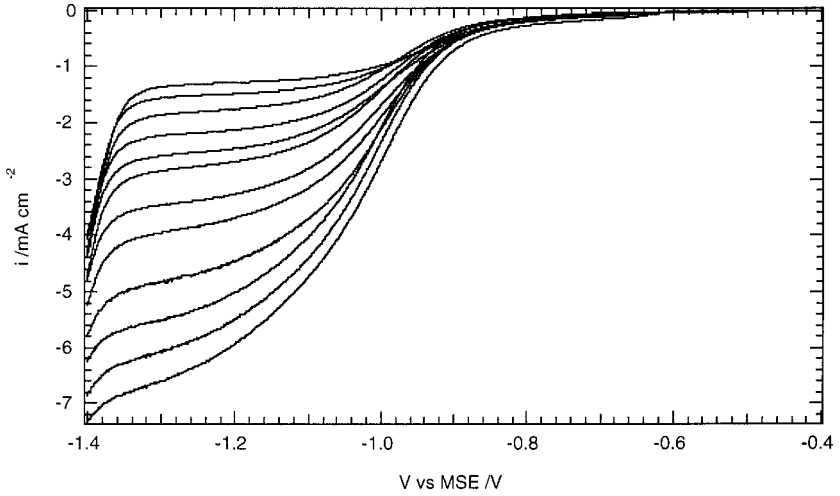

Fig. 2. Quasi-steady state polarization curves measured at 5 mV s^{-1} on a RDE at different rotation rates of 100, 150, 200, 300, 400, 500, 750, 1000, 1500, 2000, 2500 and 3000 rpm.

parameters were chosen such that the copper content of the alloys varied approximately from 5 to 30 mol % for a chosen rotation rate of the rRCE of 1000 rpm. To calculate the copper limiting current density for these conditions the diffusion coefficient of copper was derived from b_{RDE} assuming a kinematic viscosity of $v = 1.5 \times 10^{-2}$ cm^2 s^{-1}. Using these values and the copper concentration in the electrolyte the limiting current density for a given rotation rate is obtained from Equation 7 due to the Eisenberg, Tobias and Wilke [32]:

$$i_{lim} = b_{RCE}\omega^{0.7} \quad (7)$$

where $b_{RCE} = zFcD^{0.644}v^{-0.344}d^{0.4}$.

Table 4 shows the molar fraction of copper in the alloys calculated from Equations 1 and 2, respectively, together with measured values. Also indicated are the measured current efficiencies for alloy deposition. The model prediction and experimentally measured copper content as a function of off-time are shown in Figure 3. At longer off-time the measured values deviate increasingly from the predicted ones because the surface coverage of copper increasingly affects the displacement reaction. In Figure 4 the molar fractions of Fe, Co, and Cu in the alloy are presented as a function of off-time. While the Cu content increases with increasing off-time the concentration of Co and to a lesser extent of Fe decrease. This shows that with pulse-plating one can vary the ratios of Cu/Co and Fe/Co without changing the electrolyte composition or the hydrodynamic conditions.

For the subsequent experiments with the IrRDE geometry, a current efficiency of 90% was assumed based on the data in Table 4. As the sample at 20 mol % copper showed soft magnetic properties, plating parameters were selected to obtain alloys with about that composition using different pulse-parameters at a constant duty cycle of 20%. The rotation rate in these experiments was 238 rpm. A cathodic current of similar magnitude as the limiting current of copper was applied during the off-time to suppress the displacement reaction. In these conditions Cu deposits during the off-time without substantial corrosion of Fe and Co and as a consequence, it is not necessary to include the effect of deposited copper on the rate of the displacement reaction in the theoretical modeling. Model predictions and experimentally measured alloy concentrations for copper, iron and cobalt are presented in Figure 5 as a function of pulse off-time. A constant alloy composition is indeed achieved for the parameters used.

The experiments of series 2 of Table 2 were performed without applying a magnetic field to induce a uniaxial magnetic anisotropy. The deposits obtained did not give reproducible results for the magnetic field strength.

Table 3. Determination of limiting current for copper deposition at a rotation rate of 238 rpm using regression analysis at different potentials (Equation 5)

E/V vs MSE	−1.12 to −1.16	−1.17 to −1.21	−1.22 to −1.26
$(1/i_k)$/mA^{-1} cm	−0.049	−0.031	−0.021
$1/b_{RDE}$	−2.498	−2.484	−2.464
i_{lim}/mA cm^{-2}	−2.00	−2.01	−2.03

Table 4. Copper content in the deposits calculated from Equations 1 and 2, respectively, for different off-times and experimental values of current efficiency and copper content
Film thickness about 1.6 μm

t'_p /ms %	X_{Cu} (Equation 1) /mol%	X_{Cu} (Equation 2) /mol %	γ /%	X_{Cu} (experimental) /mol %
10	4.5	4.9	91.6	6.4
40	7.2	7.9	91.3	9.2
70	9.9	10.8	91.5	12.3
100	12.6	14	89.9	14.7
160	18.0	20.2	89.4	19.4
320	32.4	38.2	84.8	27.9

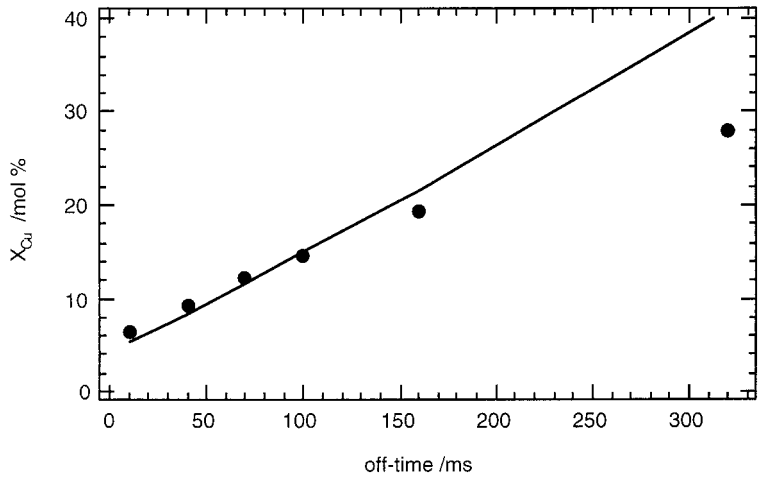

Fig. 3. Model predictions and experimental data on copper content as a function of pulse off-time at a fixed pulse on-time $t_p = 40$ ms (series 1 of Table 2).

Hence, a third set of experiments was carried out to study the effect of pulse parameters on the coercive field strength by placing a hard magnet under the substrate. The rotation rate was lowered to achieve a lower copper content in the deposits (~10 wt %). The coercive field was determined from measured *B–H* loops. No significant influence of studied pulse parameters on the easy axis coercive field strength was found, all value being 1.5 ± 0.15 Oe. No correction for the magnetic earth field was made. Several factors may be responsible for the relatively large standard deviation including uncertainties in positioning the measuring set-up perpendicular to the earth field or misalignment of the sample with respect to the magnet during deposition or in the solenoid during measurements. The observed constant values of the strongly structure dependent coercive field strength suggested that varying the pulse parameters within the range indicated did not lead to a modification of microstructure. This was confirmed by transmission electron microscopy (TEM). The samples of series 3 plated at the shortest and longest pulse off-times, respectively, had the same nanocrystalline grain structure. The nanocrystalline structure of these films which apparently is responsible for their soft magnetic properties is illustrated in Figure 6.

5. Conclusions

It has been shown that the theory previously developed for pulse plating of binary alloys can be applied to ternary alloys such as CoFeCu by considering Cu as the noble component and Co and Fe as the less noble components of a pseudo binary alloy. The simple model presented offers interesting possibilities to control the composition of ternary alloys by selecting appropriate pulse parameters. For example, the present results show one can increase the copper content of a CoFeCu alloy deposit and decrease that of iron and cobalt without changing the formulation of the electrolyte or the hydrodynamic conditions. On the other hand, alloys of identical composition can be obtained with different

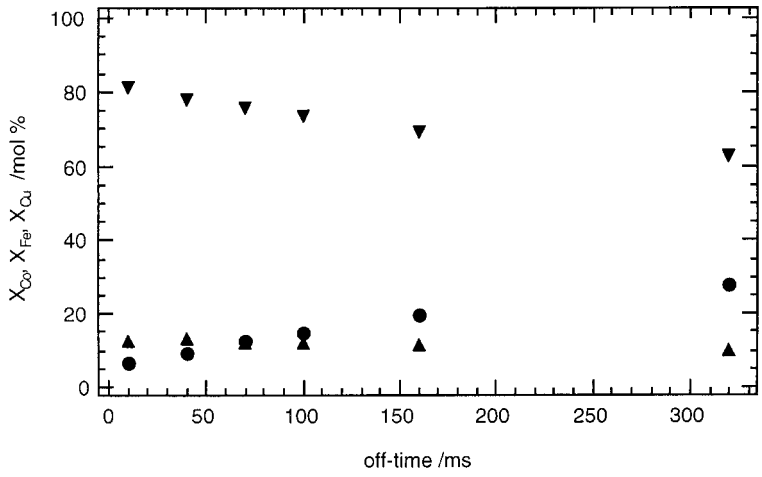

Fig. 4. Cobalt, iron and copper content in the deposit as a function of pulse off-time at a fixed pulse on-time $t_p = 40$ ms (series 1 of Table 2). Key: (▼) X_{Co}, (▲) X_{Fe} and (●) X_{Cu}.

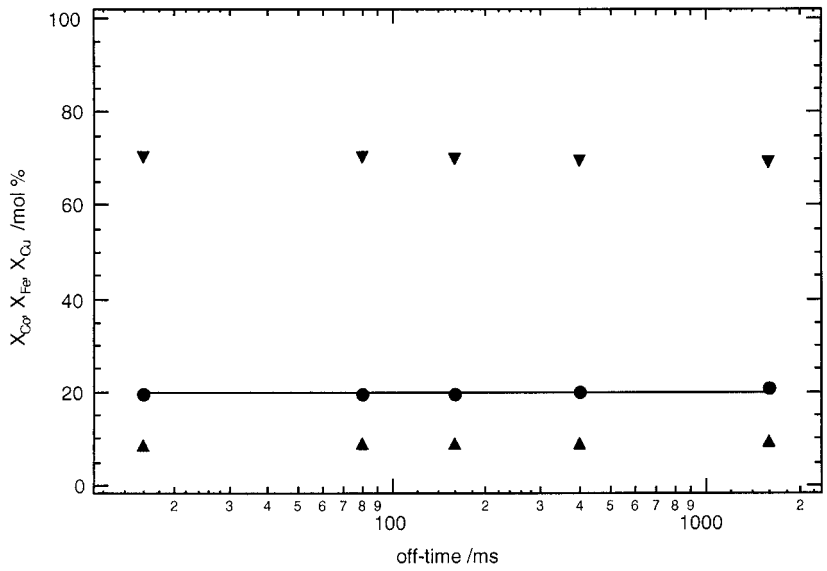

Fig. 5. Model predictions and experimental data for cobalt, iron and copper content of deposits pulse plated at a fixed duty cycle of 20% for different of pulse off-times (series 2 of Table 2). Key: (▼) X_{Co}, (▲) X_{Fe}, (●) X_{Cu} and (—) $X_{Cu,theoretical}$.

pulse parameters. This offers the possibility to influence microstructure by changing pulse parameters. For CoFeCu alloys in the range of pulse parameters investigated here, no effect of pulse parameters on the structure sensitive magnetic coercive field strength was observed, however. Indeed, all deposits formed in a series of experiments with constant alloy composition had the same nanocrystalline grain structure. More studies are needed to better understand the effect of pulse parameters on the structure of electroplated functional alloy films.

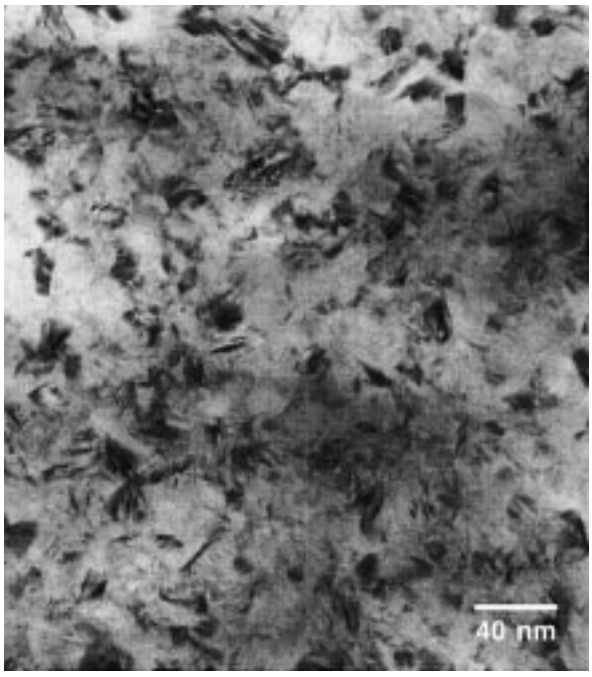

Fig. 6. Transmission electron micrograph (plain view) showing the nanocrystalline structure of a film plated at 1600 ms pulse off-time. Same structure was observed for an off-time of 16 ms (series 3 of Table 2).

Acknowledgements

The authors thank J.J. Kelly for TEM analysis and the machine shop of the Materials Department for fabricating the electrochemical cells and electrodes. This work was financially supported by Fonds National Suisse de la Recherche Scientifique, Bern.

References

1. F. Pfeifer and C. Radeloff, *J. Magn. Magn. Mat.* **19** (1980) 190.
2. S.H. Liao, *IEEE Trans. Magn.* **MAG23** (1987) 2981.
3. S.H. Liao and C.H. Tolman, *US Patent 4 756 816*, 12 July (1988).
4. C.H. Tolman, *J. Appl. Phys.* **38** (1967) 3409.
5. G. Herzer, 'Handbook of Magnetic Materials', Vol. 10, (Elsevier Science, 1997), Chap. 3, p. 415.
6. Yu.A. Durasova and N.T. Nikitina, *Izr. Akad. Nauk. USSR*, serie Fizika XXIX (1965) 557.
7. L.T. Romankiw and D.A. Thompson, 'Properties of Electrodeposits, Their Measurement and Significance' (The Electrochemical Society, Penington, NJ, 1976), Chap. 23, p. 407.
8. N.C. Anderson and R.B. Chesnutt, *US Patent 4 661 216*, 28 Apr. (1987).
9. J.W. Chang, P.C. Andricacos, B. Petek and L.T. Romankiw, Proc. First International Symposium on 'Magnetic Materials, Processes and Devices', Vol. 90-8, The Electrochemical Society, Hollywood, FA (1989), p. 361.
10. S.H. Liao, *US Patent 5 168 410*, 1 Dec. (1992).
11. T. Osaka, 194th Meeting of The Electrochemical Society, Vol. 98-2, Boston MA Nov. (1998), Abstract 487.
12. M. Takai, K. Hayashi, M. Aoyagi and T. Osaka, *J. Electrochem. Soc.* **144** (1997) L203.
13. J.W. Chang, P.C. Andricacos, B. Petek and L.T. Romankiw, Proc. Second International Symposium on 'Magnetic Materials, Processes and Devices', Vol. 92-10, The Electrochemical Society, Phoenix, AZ (1991), p. 275.

14. J.W. Chang, P.C. Andricacos and L.T. Romankiw, Proc. Second International Symposium, ref. [13], p. 315.
15. P.C. Andricacos and N. Robertson, *IMB J. Res. Develop.* **42** (1998) 671.
16. J.W. Chang, P.C. Andricacos, B. Petek, P.T. Troilloud and L.T. Romankiw, 194th Meeting of The Electrochemical Society, ref. [11], Abstract 488.
17. G. Poupon, 194th Meeting of The Electrochemical Society, ref. [11], Abstract 490.
18. T. Osaka, M. Takai, K. Hayashi, K. Ohashi, M. Saito and K. Yamada, *Nature* **392** (1998) 796.
19. T. Osaka, 194th Meeting of The Electrochemical Society, ref. [11], Abstract 491.
20. Y. Omata and N. Kaminaka, Proc. Second International Symposium, ref. [13], p. 255.
21. J.-M. Maire and G. Poupon, 194th Meeting of The Electrochemical Society, ref. [11], Abstract 491.
22. S. Roy, M. Matlosz and D. Landolt, *J. Electrochem. Soc.* **141** (1994) 1509.
23. S. Roy and D. Landolt, *J. Electrochem. Soc.* **142** (1995) 3021.
24. P.E. Bradley, S. Roy and D. Landolt, *J. Chem. Soc., Trans. Farad.* **92** (20) (1996) 4015.
25. P.E. Bradley and D. Landolt, *Electrochim. Acta* **42** (1997) 993.
26. P.E. Bradley, Thesis no. 1785, EPFL Lausanne (1998).
27. P.E. Bradley and D. Landolt, *Electrochim. Acta* **45** (1999) 1077.
28. P.E. Bradley, D. Landolt and W.E. Bradley, *Swiss Patent Appl. CF/1996 1683/96*.
29. P.E. Bradley and D. Landolt, *J. Electrochem. Soc.* **144** (1997) L145.
30. A.J. Bard and L.R. Faulkner, 'Electrochemical Methods, Fundamentals and Applications' (J. Wiley & Sons, New York), p. 291.
31. W.G. Levich, 'Physichochemical Hydrodynamics' (Prentice-Hall, Englewoods Cliffs, NJ, 1962), p. 60.
32. M. Eisenberg, C.W. Tobias and C.R. Wilke, *J. Electrochem. Soc.* **101** (1954) 306.